Analysis of Heat Transfer Regulation and Modification Employing Intermittently Emplaced Porous Cavities

K. Vafai
Professor.
Fellow ASME

P. C. Huang

Department of Mechanical Engineering,
The Ohio State University,
Columbus, OH 43210

The present work forms a fundamental investigation on the effects of using intermittently porous cavities for regulating and modifying the flow and temperature fields and therefore changing the skin friction and heat transfer characteristics of an external surface. A general flow model that accounts for the effects of the impermeable boundary and inertial effects is used to describe the flow inside the porous region. Solutions of the problem have been carried out using a finite-difference method through the use of a stream function-vorticity transformation. Various interesting characteristics of the flow and temperature fields in the composite layer are analyzed and discussed in detail. The effects of various governing dimensionless parameters, such as the Darcy number, Reynolds number, Prandtl number, the inertia parameter as well as the effects of pertinent geometric parameters are thoroughly explored. Furthermore, the interactive effects of the embedded porous substrates on skin friction and heat transfer characteristics of an external surface are analyzed. The configuration analyzed in this work provides an innovative approach in altering the frictional and heat transfer characteristics of an external surface.

Introduction

Forced convection heat transfer through porous media has been a major topic for various studies during the past decades due to many engineering applications such as thermal insulation engineering, water movements in geothermal reservoirs, underground spreading of chemical waste, nuclear waste repository, grain storage, and enhanced recovery of petroleum reservoirs (Tien and Vafai, 1989; De Vries, 1958). The majority of the previous investigations include flow through a semi-infinite porous medium for external boundaries, and flow through structures that are fully filled with the porous medium for internal flows. However, consideration of the interaction between the porous-saturated region and the fluid region did not form a part of most of these studies due to the difficulties in simultaneously solving the coupled momentum equations for both porous and fluid regions. There has been very little work done on these types of interactions, which can occur in various practical applications. Furthermore, many of the existing studies on convective heat transfer in porous media are based on the Darcy's law, which is found to be inadequate for the formulation of fluid flow and heat transfer problems in porous media when there is an impermeable boundary and/or the Reynolds number based on the pore size is greater than unity.

A general theory and numerical calculation techniques for flow field and heat transfer in recirculating flow without including the porous medium have been developed by Gosman (1976), and were successfully used by various investigators such as Gooray (1982) and Gooray et al. (1981, 1982). They have shown that these methods can be applied to give reasonably accurate quantitative heat transfer results for the separated forced convection behind a backstep. A few studies have been reported on forced convection in a rectangular cavity. Yamamoto et al. (1979) experimentally studied the forced convection on a heated bottom surface of a cavity situated on a duct wall. They have shown that reattachment of separated flow for shallow cavities and vortex flow for deeper ones had a large effect on the heat transfer behavior on the heated bottom surface. Sinha et al. (1981) reported the experimental results for laminar separating flow over backsteps and cavities. They found that cavities can be classified as closed, shallow open, and open depending on the range of the value of the aspect (depth-width) ratio. Aung (1983) performed an experimental investigation of separated forced convection laminar flow past two-dimensional rectangular cavities where the walls are kept at a constant temperature. He found that the temperature distribution outside of the cavity had little influence on the flow in the cavity and the local heat transfer distribution on the cavity floor attains a maximum value that is located between the midpoint of the cavity floor and the downstream wall.

Bhatti and Aung (1984) numerically examined the laminar separated forced convection in the cavities. They found that the average Nusselt number in open cavity flow is related to the Reynolds number raised to a power that depends on the aspect ratio of the cavity and that the influence of the upstream boundary layer thickness on the heat transfer in the cavity is negligible. Most of the existing related studies on convection in composite systems were focused on the problem of natural convection in an enclosure (Beckermann et al., 1988; Bejan, 1984; Sathe et al., 1988; Cheng, 1978; Poulikakos and Bejan, 1985) or forced convection in a duct (Poulikakos and Kazmierczak, 1987; Bejan, 1984), or external and internal boundaries (Vafai and Kim, 1990; Poulikakos, 1986; Bejan, 1984). However, to the best of the author's knowledge, there have not been any investigations on the forced convection over porous cavities in the open literature.

The present work constitutes one of the first analyses of the separated forced convection through porous cavities. The pre-

Contributed by the Heat Transfer Division for publication in the JOURNAL OF HEAT TRANSFER. Manuscript received by the Heat Transfer Division September 1992; revision received August 1993. Keywords: Materials Processing and Manufacturing Processes, Porous Media, Thermal Packaging. Associate Technical Editor: C. E. Hickox, Jr.

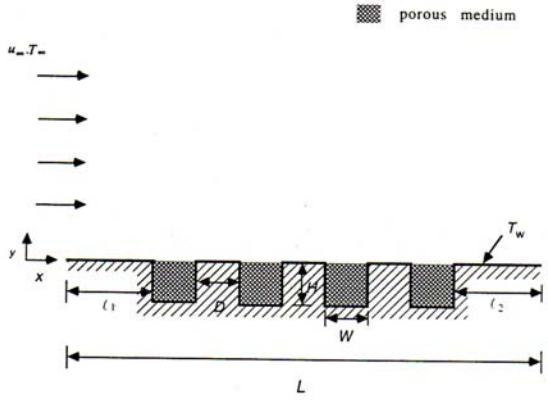

Fig. 1 Schematic diagram of flow and heat transfer over intermittently emplaced porous cavities

sent investigation provides a valuable fundamental framework for predicting heat transfer and fluid flow characteristics for other composite systems. The results and fundamental information presented here along with those analyzed by Huang and Vafai (1993) can be extended to examine various applications such as in electronic cooling and in heat exchanger design, reduction of skin friction and heat transfer enhancement or augmentation, some of the manufacturing processes, geothermal reservoirs, and oil extraction. In addition, the present work constitutes an innovative way of regulating and modifying the skin friction and heat transfer characteristics of an external surface.

Analysis and Formulation

The configuration for this problem is shown in Fig. 1. The height and width of the porous cavities are H and W, respectively, the distance between two cavities is D, the length of the wall is L, the free-stream velocity is u_∞, and the free-stream temperature is T_∞. The wall is maintained at a constant temperature T_w. It is assumed that the flow is steady, laminar, incompressible, and two dimensional. In addition, the thermophysical properties of the fluid and the porous matrix are assumed to be constant and the fluid-saturated porous medium is considered homogeneous and isotropic and in local thermodynamic equilibrium with the fluid. For the fluid region the conservation equations for mass, momentum, and energy are

$$\nabla \cdot \mathbf{v} = 0 \tag{1}$$

$$\mathbf{v} \cdot \nabla \mathbf{v} = -\frac{1}{\rho_f} \nabla P + \nu_f \nabla^2 \mathbf{v} \tag{2}$$

$$\mathbf{v} \cdot \nabla T = \alpha_f \nabla^2 T \tag{3}$$

Based on the Brinkman-Forchheimer-extended Darcy model, which accounts for the effects of the inertial and impermeable boundary, the mass, momentum and energy equations in the porous matrix (Vafai and Tien, 1981, 1982) can be expressed as

$$\nabla \cdot \mathbf{v} = 0 \tag{4}$$

$$\mathbf{v} \cdot \nabla \mathbf{v} = -\frac{1}{\rho_f} \nabla P + \nu_{\text{eff}} \nabla^2 \mathbf{v} - \left(\frac{\nu_{\text{eff}}}{K} + \frac{F\epsilon}{\sqrt{K}} |\mathbf{v}| \right) \mathbf{v} \tag{5}$$

$$\mathbf{v} \cdot \nabla T = \alpha_{\text{eff}} \nabla^2 T \tag{6}$$

where K and ϵ are the porous medium's permeability and porosity, and ν_{eff} and α_{eff} are the effective kinematic viscosity and thermal conductivity of the porous medium. It should be noted that velocity $\mathbf{v}$ and temperature T in the porous region are both volume-averaged quantities as described by Vafai and Tien (1981). The boundary conditions necessary to complete the problem formulation are

$$u = u_\infty, \quad v = 0, \quad P = P_\infty, \quad T = T_\infty \quad \text{at} \quad x = 0 \tag{7}$$

$$u = 0, \quad v = 0, \quad T = T_w \quad \text{on all solid walls} \tag{8}$$

$$u = u_\infty, \quad P = P_\infty, \quad T = T_\infty \quad \text{as } y \to \infty \tag{9}$$

In addition to these, the two sets of conservation equations are coupled by the following matching conditions at the porous/fluid interface:

$$u|_{y=H^-} = u|_{y=H^+}, \quad v|_{y=H^-} = v|_{y=H^+} \tag{10a}$$

$$P|_{y=H^-} = P|_{y=H^+}, \quad \mu_{\text{eff}} \frac{\partial v}{\partial y}\bigg|_{y=H^-} = \mu_f \frac{\partial v}{\partial y}\bigg|_{y=H^+} \tag{10b}$$

$$\mu_{\text{eff}} \left(\frac{\partial u}{\partial y} + \frac{\partial v}{\partial x} \right)\bigg|_{y=H^-} = \mu_f \left(\frac{\partial u}{\partial y} + \frac{\partial v}{\partial x} \right)\bigg|_{y=H^+} \tag{10c}$$

$$T|_{y=H^-} = T|_{y=H^+}, \quad k_{\text{eff}} \frac{\partial T}{\partial y}\bigg|_{y=H^-} = k_f \frac{\partial T}{\partial y}\bigg|_{y=H^+} \tag{10d}$$

Nomenclature

A = dimensionless geometric parameter = W^*/H^*
B = dimensionless geometric parameter = D^*/H^*
C_f = friction coefficient
D = spacing between the porous cavities, m^{-1}
Da_L = Darcy number = K/L^2
F = a function used in expressing inertia terms
h = convective heat transfer coefficient, $Wm^{-2}K^{-1}$
H = thickness of the porous medium, m
k = thermal conductivity, $Wm^{-2}K^{-1}$
K = permeability of the porous medium, m^2
ℓ_1 = length of plate upstream from the cavities, m
ℓ_2 = length of plate downstream from the cavities, m
L = length of the external boundary as shown in Fig. 1, m
N = number of cavities
Nu = Nusselt number = hx/k_f
P = pressure, Pa
Pe_L = Peclet number = $u_\infty L/\alpha$
Pr = Prandtl number = ν/α
Re = Reynolds number = $u_\infty L/\nu$
S^Φ = source term, used in Eq. (24)
T = temperature, K
u = x-component velocity, ms^{-1}
v = y-component velocity ms^{-1}
$\mathbf{v}$ = velocity vector, ms^{-1}
W = width of the porous cavity, m
x = horizontal coordinate, m
y = vertical coordinate, m
α = thermal diffusivity, m^2s^{-1}
α_{eff} = effective thermal diffusivity = $k_{\text{eff}}/\rho_f c_{p,f}$, m^2s^{-1}
ϵ = porosity of the porous medium
θ = dimensionless temperature = $(T - T_\infty)/(T_w - T_\infty)$
Λ_L = inertial parameter = $FL\epsilon/\sqrt{K}$
μ = dynamic viscosity, $kgm^{-1}s^{-1}$
ν = kinematic viscosity, m^2s^{-1}
ξ = vorticity
ρ = fluid density, kgm^{-3}
Φ = transported property; general dependent variable
ψ = stream function

Superscripts

* = dimensionless quantity

Subscripts

eff = effective
f = fluid
∞ = condition at infinity

Vorticity-Stream Function Formulation. The governing equations above are cast in terms of the vorticity-stream formulation. Introducing stream function and vorticity as

$$u=\frac{\partial\psi}{\partial y},\quad v=-\frac{\partial\psi}{\partial x} \tag{11}$$

$$\xi=\frac{\partial v}{\partial x}-\frac{\partial u}{\partial y} \tag{12}$$

the governing equations for the whole region can be expressed in dimensionless form as

$$\frac{\partial\psi^*}{\partial y^*}\frac{\partial\xi^*}{\partial x^*}-\frac{\partial\psi^*}{\partial x^*}\frac{\partial\xi^*}{\partial y^*}=\frac{1}{\mathrm{Re}_L}\nabla^2\xi^*+S^* \tag{13}$$

$$\nabla^2\psi^*=-\xi^* \tag{14}$$

$$\frac{\partial\psi^*}{\partial y^*}\frac{\partial\theta}{\partial x^*}-\frac{\partial\psi^*}{\partial x^*}\frac{\partial\theta}{\partial y^*}=\nabla\cdot\left(\frac{1}{\mathrm{Pe}_L}\nabla\theta\right) \tag{15}$$

where in the fluid region

$$\mathrm{Re}_L=\frac{u_\infty L}{\nu_f},\quad \mathrm{Pe}_L=\frac{u_\infty L}{\alpha_f},\quad S^*=0 \tag{16a}$$

and in the porous region

$$\mathrm{Pe}_L=\frac{u_\infty L}{\alpha_{\mathrm{eff}}},\quad \mathrm{Da}_L=\frac{K}{L^2},\quad \Lambda_L=\frac{FL\epsilon}{K^{1/2}} \tag{16b}$$

$$S^*=-\frac{1}{\mathrm{Re}_L\mathrm{Da}_L}\xi^*-\Lambda_L|\mathbf{v}^*|\xi^*-\Lambda_L\left(v^*\frac{\partial|\mathbf{v}^*|}{\partial x^*}-u^*\frac{\partial|\mathbf{v}^*|}{\partial y^*}\right)+\frac{u^*}{\mathrm{Re}_L}\frac{\partial}{\partial y^*}\left(\frac{1}{\mathrm{Da}_L}\right)-\frac{v^*}{\mathrm{Re}_L}\frac{\partial}{\partial x^*}\left(\frac{1}{\mathrm{Da}_L}\right)+|\mathbf{v}^*|u^*\frac{\partial}{\partial y^*}(\Lambda_L)-|\mathbf{v}^*|v^*\frac{\partial}{\partial x^*}(\Lambda_L) \tag{17}$$

the dimensionless boundary conditions thus become

$$\psi^*=y^*,\quad \xi^*=-\frac{\partial^2\psi^*}{\partial x^{*2}},\quad \theta=0,\ \text{at } x^*=0 \tag{18}$$

$$\psi^*=0,\quad \xi^*=-\frac{\partial^2\psi^*}{\partial x^{*2}},$$

$$\theta=1,\ \text{at } x^*=\begin{cases}l_1^*+(N-1)(W^*+D^*)\\ l_1^*+NW^*+(N-1)D^*\end{cases},\quad 0>y^*>-H^* \tag{19}$$

$$\psi^*=0,\quad \xi^*=-\frac{\partial^2\psi^*}{\partial y^{*2}},\quad \theta=1,$$

$$\text{at } x^*=\begin{cases}l_1^*+(N-1)(W^*+D^*)<x^*<l_1^*+NW^*+(N-1)D^*,\ y^*=-H^*\\ 0<x^*<l_1^*\\ l^*+NW^*+(N-1)D<x^*<l_1^*+NW^*+ND^*\\ (1-l_2^*)<x^*<1\end{cases},\qquad y^*=0 \tag{20}$$

$$\frac{\partial\psi^*}{\partial y^*}=1,\quad \xi^*=-\frac{\partial^2\psi^*}{\partial x^{*2}},\quad \theta=0,\ \text{as } y^*\to\infty \tag{21}$$

where N (= 1, 2, 3, 4) is the number of porous cavities. Note that the variables in the equations above are defined as follows:

$$x^*=\frac{x}{L},\quad y^*=\frac{y}{L},\quad u^*=\frac{u^*}{u_\infty},\quad v^*=\frac{v}{u_\infty},\quad \mathbf{v}^*=\sqrt{u^{*2}+v^{*2}} \tag{22a}$$

$$\psi^*=\frac{\psi}{u_\infty L},\quad \xi^*=\frac{L\xi}{u_\infty},\quad \theta=\frac{T-T_\infty}{T_w-T_\infty} \tag{22b}$$

$$H^*=\frac{H}{L},\quad l_1^*=\frac{l_1}{L},\quad l_2^*=\frac{l_2}{L},\quad D^*=\frac{D}{L},\quad W^*=\frac{W}{L} \tag{22c}$$

From the equations above, boundary conditions, and geometry arrangement of cavities given above it is seen that the present problem is governed by seven dimensionless parameters. These are Darcy, Reynolds, and Prandtl numbers, the inertia parameter, the number of cavities N, and the geometry parameters A and B, where

$$A=\frac{W^*}{H^*},\quad B=\frac{D^*}{H^*}. \tag{23}$$

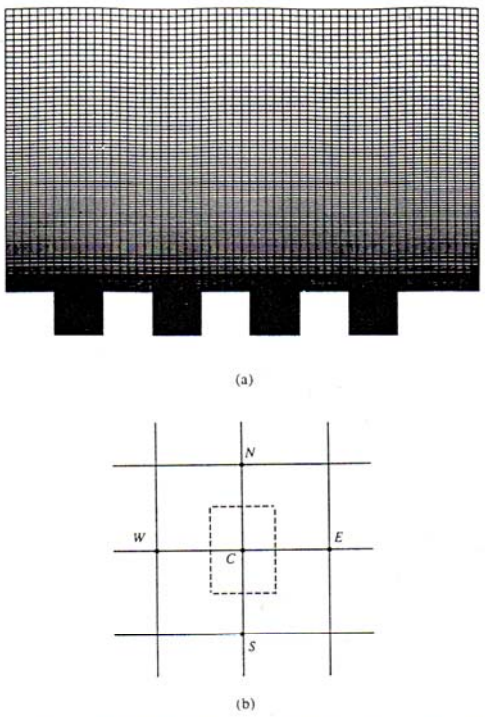

Fig. 2 *(a)* **The nonuniform grid system for the whole computational domain;** *(b)* **local integration cell in the computational domain**

Numerical Scheme and Stability and Accuracy Considerations

Employing a nonuniform rectangular grid system, the finite-difference form of the vorticity transport, stream function, and energy equations were derived using control-volume integration of these differential equations over discrete cells surrounding the grid points, as shown in Fig. 2. In the above discretization scheme the upwind and central-differencing formats are also introduced for the convective and diffusive terms, respectively. This results in a system of equations of the following form:

$$C_C\Phi_C=C_N\Phi_N+C_S\Phi_S+C_E\Phi_E+C_w\Phi_W+S^\Phi \tag{24}$$

where Φ stands for the transported variables, Cs are coefficients combining convective and diffusive terms, and S^Φ is the appropriate source term. The subscripts on C denote the main grid points surrounded by the four neighboring points denoted as N, S, E, and W.

To ensure the continuity of the diffusive and convective fluxes across the interface without requiring the use of an excessively fine grid structure, the harmonic mean formulation suggested by Patankar (1980) was used to handle abrupt changes in thermophysical properties, such as the permeability and the thermal conductivity, across the interface. Moreover, the source terms incorporated with the boundary and inertia effects were linearized as described by Patankar (1980). The vorticity at sharp corners requires special consideration. Seven different methods of handling this corner vorticity are discussed by Roache (1976). Here average treatment for the evaluation of vorticity suggested by Greenspan (1969) is used to model the mathematical limit of a sharp corner as appropriately as possible.

The finite difference equations thus obtained were solved by the extrapolated-Jacobi scheme. This iterative scheme is based on a double cyclic routine, which translates into a sweep of only half of the grid points at each iteration step (Adams and Ortega, 1982). In this work convergence was considered to have been achieved when the absolute value of relative error on each grid point between two successive iterations was found to be less than 10^{-6}. The iterative procedure was then terminated. To examine the independence of the results on the chosen Δx and Δy, many numerical runs with different combinations of Δx and Δy were performed. This was done by a systematic decrease in the grid size until further refinement of the grid size resulted in less than 1 percent difference in the converged results. A grid size of 162×188 was finally found to model accurately the flow field described in the results for all the considered cases. The application of the boundary condition at infinity, at a finite distance from the wall was given careful consideration. This was done through the following procedure. The length of the computational domain in the vertical direction was systematically increased until the maximum vorticity changes for two consecutive runs would become less than 1 percent. Therefore, in our investigation the computational domain is chosen to be larger than the physical domain.

Along the x direction, the computational domain starts at a distance of one-fifth of total length upstream, i.e., L, of the physical domain. This procedure eliminates the errors associated with the singular point at the leading edge of the composite system. On the other side, the computational domain is extended over a distance of two-fifths of the total length downstream from the trailing edge of the physical domain. Since the present problem has a significant parabolic character, the downstream boundary condition on the computational domain does not have much influence on the physical domain. In the y direction the computational domain is extended up to a distance sufficient enough to ensure that even for the smallest value of the Reynolds number the upper boundary lies well outside the boundary layer through the entire domain. In the present study locating the upper boundary at a distance of eight times the depth of the cavity has been found to be sufficient. Extensions beyond eight times the depth of the cavity had no effect on the solution.

To validate the numerical scheme used in the present study, initial calculations were performed for laminar flow over a flat plate (i.e., $H^* = 0$, for no porous substrate) and that over a flat plate embedded in a porous medium (i.e., $H^* \to \infty$ and $W^* \to \infty$, representing the full porous medium case). The results for $H^* = 0$ agree to better than 1 percent with boundary layer similarity solutions for velocity and temperature fields. The results for $H^* \to \infty$ and $W^* \to \infty$ agree extremely well with data reported by Vafai and Thiyagaraja (1987) and Beckermann et al. (1987).

Results and Discussion

The effects of the geometric arrangements of the porous cavities as well as the effects of different values of Ra_L, Da_L, Pr, and Λ_L on the flow and temperature fields were investigated. Table 1 displays various input parameter sets considered in this analysis. The parameter sets presented in Table 1 were only a subset of much larger set that was investigated in this work. The parameter sets presented in Table 1 were found to be most important in revealing pertinent aspects of the geometric arrangements of the porous cavities and variations in the thermophysical properties. Figures 3–12 show streamlines and isotherms over multiple porous cavities for the corresponding cases listed in Table 1. To illustrate the results of flow and temperature fields inside the porous cavity, only the portion that concentrates on the porous/fluid region and its close vicinity is presented. However, it should be noted that the computational domain included a significantly larger region than what is displayed in the subsequent figures. Furthermore, for brevity some figures are not shown here.

Table 1 Input data of governing parameters for intermittently emplaced cavities

Case #	Re_L	Da_L	Pr	Λ_L	A	B	N
1	3×10^5	8×10^{-6}	0.7	0.35	6	1	4
2	2×10^5	8×10^{-6}	0.7	0.35	6	1	4
3	3×10^5	8×10^{-4}	0.7	0.35	6	1	4
4	3×10^5	8×10^{-6}	7	0.35	6	1	4
5	3×10^5	8×10^{-6}	100	0.35	6	1	4
6	3×10^5	8×10^{-6}	0.7	1.05	6	1	4
7	3×10^5	8×10^{-6}	0.7	0.35	3	1	4
8	3×10^5	8×10^{-6}	0.7	0.35	6	0.8	4
9	3×10^5	8×10^{-6}	0.7	0.35	3	2	4
10	3×10^5	8×10^{-6}	0.7	0.35	12.5	1	2

Effect of the Reynolds Number. Figure 3 shows streamlines and isotherms over four porous cavities with $A = 6$ and $B = 1$ for the case where $Pr = 0.7$, $\Lambda_L = 0.35$, $Da_L = 8 \times 10^{-6}$, and $Re_L = 3 \times 10^5$. It can be seen that a laminar vortex resides within each of these cavities. The strength of the eddies within each cavity decreases farther along the flow direction. These recirculating flows are formed as the primary flow impinges on the downstream cavity wall and then flows toward the bottom surface. Due to an increase in the thickness of external boundary layer along the plate, there is a reduction in the mass flow rate that penetrates into each subsequent cavity. This in turn causes a reduction in the strength of vortices within the cavities as the flow moves farther downstream. Figure 3(*a*) also shows that within each cavity the streamlines between the vortex center and the downstream wall of that cavity are denser than those between the vortex center and the upstream wall of the cavity. This is because the magnitude of the downstream vertical velocity is larger than the upstream one. The small fluctuations of the porous/fluid interfacial streamline are due to the macroscopic shear frictional resistance at the interface. As the Reynolds number decreases from 3×10^5 to 2×10^5, the center of the vortex for each cavity moves further to the left as seen in Fig. 4.

The reason for this trend is that the lower the Reynolds number, the lower the momentum of the flow, which in turn results in lower bulk frictional resistance for the flow. As a result the size of the vortex formed in the cavity increases. It should be noted that even though the increase in the increase in the size of the vortex is small, nevertheless, through careful examination of the results it can be clearly observed. Comparison of the isotherms in Figs. 3(*b*) and 4(*b*) indicates that at a smaller Reynolds number, due to the larger size of the vortex, the isotherms penetrate farther inside the cavity.

To evaluate the effects of the intermittent porous cavities on the shear stress and heat transfer rate at the wall, additional calculations were carried out. For the shear stress the results were cast in dimensionless form by means of the local friction coefficient as

$$C_f = \frac{\tau_{w,x}}{\rho_f u_\infty^2/2} = \frac{2}{\mathrm{Re}_L} \left.\frac{\partial u^*}{\partial y^*}\right|_{y^*=0}$$

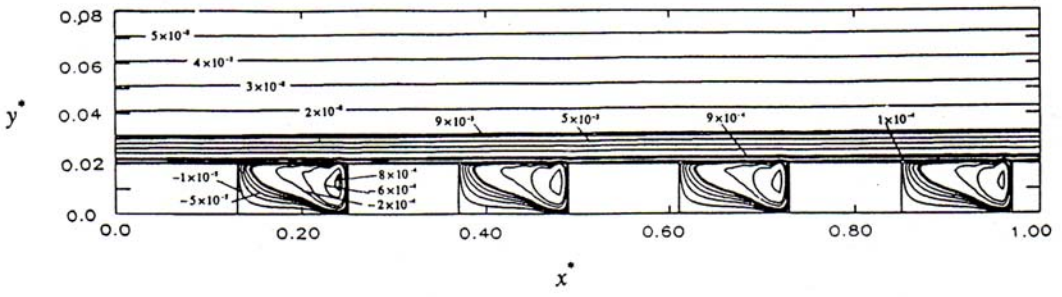

(a)

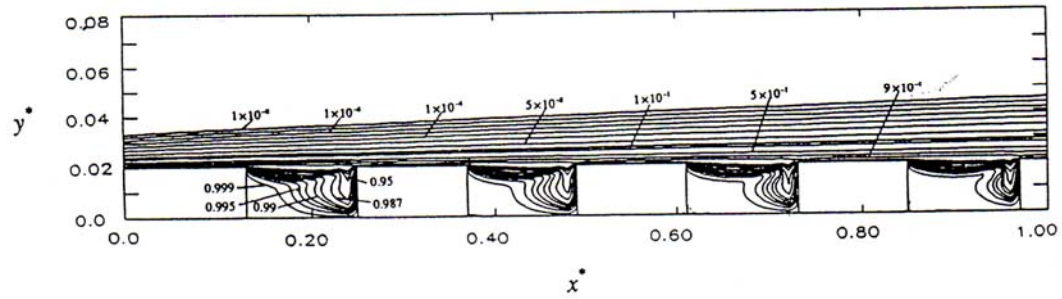

(b)

Fig. 3 (*a*) Streamlines and (*b*) isotherms for flow over four obstructing porous cavities for $Re_L = 3 \times 10^5$, $Da_L = 8 \times 10^{-6}$, $\Lambda_L = 0.35$, $Pr = 0.7$, $k_{eff}/k_f = 1.0$, $A = 6$, $B = 1$

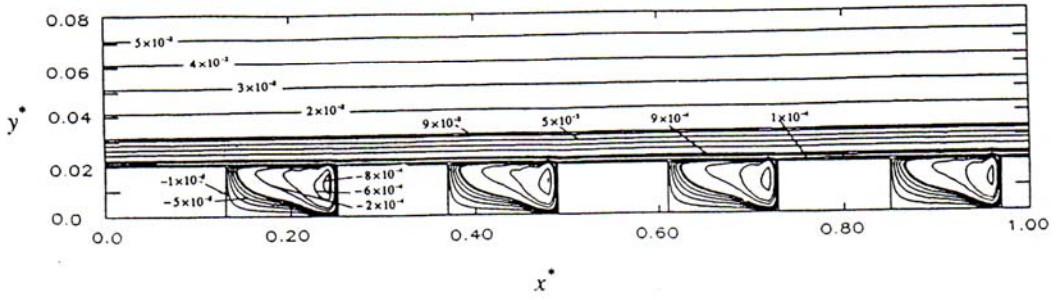

(a)

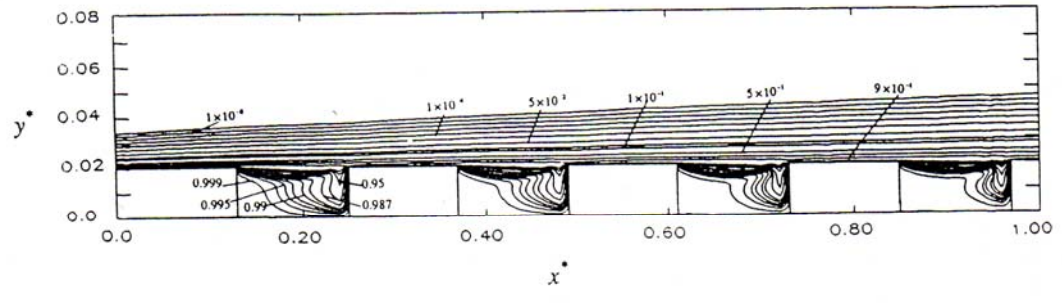

(b)

Fig. 4 (*a*) Streamlines and (*b*) isotherms for flow over four obstructing porous cavities for $Re_L = 2 \times 10^5$, $Da_L = 8 \times 10^{-6}$, $\Lambda_L = 0.35$, $Pr = 0.7$, $k_{eff}/k_f = 1.0$, $A = 6$, $B = 1$

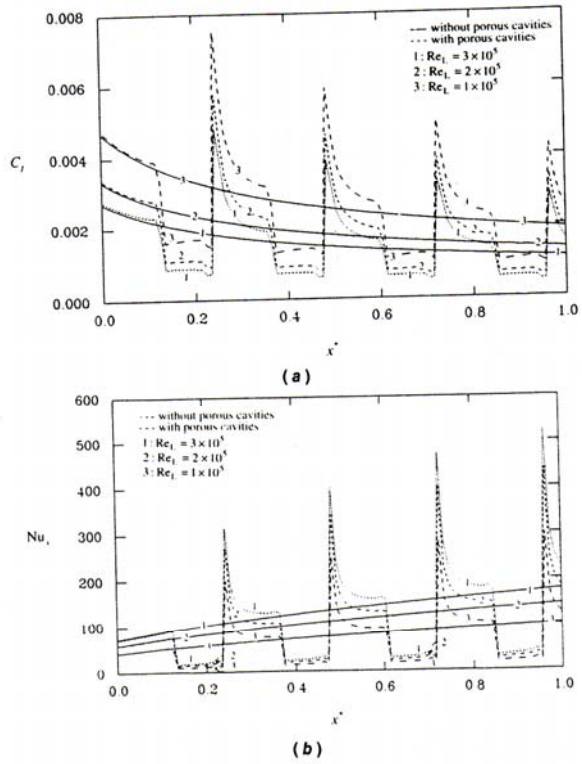

Fig. 5 Effects of the Reynolds number on (*a*) friction coefficient and (*b*) Nusselt number for flow through alternate porous cavity-block obstacles for $Da_L = 8\times10^{-6}$, $\Lambda_L = 0.35$, $Pr = 0.7$, $k_{eff}/k_f = 1.0$, $A = 3$, $B = 1$, $H^* = 0.02$

and for the heat transfer rate the results were presented in dimensionless form in terms of dimensionless Nusselt number

$$Nu_x = \frac{hx}{K_f} = -x^* \frac{k_e}{k_f} \frac{\partial\theta}{\partial y^*}\bigg|_{y^*=0} \tag{26}$$

This results in more meaningful comparisons for the heat flux at the external boundary between the composite system and the case where there were no porous obstacles. The effect of Reynolds number on friction coefficient along the wall ($y^* = 0$) is shown in Fig. 5(*a*). It can be seen that local friction coefficient fluctuates periodically as the streamwise coordinate increases due to the presence of the porous cavity obstacles, with a decreasing mean. This decrease in local friction coefficient is to a greater extent at the inlet of each porous cavity due to the nonzero velocity at this porous/fluid interface, which is different from the decrease at the impermeable solid wall. In addition, the peak in each cycle occurs at an x^* value corresponding to the right corner of each corner. This is due to a very steep velocity gradient in the fluid as it turns around the right corner of the cavities. Passing the right corner of the porous cavity, a secondary boundary layer begins at the leading edge of intercavity wall. The values of the C_f decrease again along the intercavity wall. As expected, as the Reynolds number increases, the friction coefficient and its fluctuation along the wall decreases.

Figure 5(*b*) shows the effect of Reynolds number on the Nusselt number distribution along the wall ($y^* = 0$). A periodically fluctuating variation of Nusselt number along the wall is observed with an increasing mean. At the inlet of each porous cavity, spacing between isotherms is large (see Figs. 3(*b*) or 4(*b*)), indicating a region of low temperature gradient. Therefore, the local Nusselt number reduces to a trough at the permeable wall. As the fluid turns around the right corner of each porous cavity, the Nusselt number reaches a peak because of the steep velocity gradient, which increases the heat transfer by convection. As can be seen in Fig. 5(*b*), the maximum and minimum values of Nu_x in each cycle increase as the Reynolds number increases. This is due to the higher velocities near the wall for larger Reynolds number, resulting in an increase in the transfer of convective energy.

Effect of the Darcy Number. The Darcy number $Da_L = K/L^2$ is directly related to the permeability of the porous medium. Figures 3 and 6 show the streamlines and isotherms for $Re_L = 3\times10^5$, $\Lambda_L = 0.35$, $Pr = 0.7$, $A = 6$, and $B = 1$ but with $Da_L = 8\times10^{-6}$ and 8×10^{-8}, respectively. Comparison of the streamlines in Figs. 3(*a*) and 6(*a*) shows that as the Darcy number decreases, the size of the vortices is reduced. This is because smaller values of Da_L translate into larger bulk frictional resistance for the flow in the porous medium. This in turn reduces the extent of penetration of the primary flow into the cavity. Comparison of the isotherms in Figs. 3(*b*) and 6(*b*) depicts that for the lower Darcy number case the isotherms penetrate deeper inside the cavity, especially in the left half section of cavity. The reason for this interesting effect is that for a lower Darcy number, heat diffusion is more significant than heat convection in the porous region. Note that in this study the conductivity of the porous medium is taken to be equal to that of the fluid, to concentrate on the effects of the geometric and thermophysical variations.

The effects of Darcy number on the variation of friction coefficient and local Nusselt number are depicted in Figs. 7(*a*) and 7(*b*), respectively. The fluctuating features for these two distributions (C_f and Nu_x) along the wall were given previously when the effects of the Reynolds number were discussed. As can be seen in Fig. 7(*a*), the values of C_f at the inlet of cavity increase with a decrease in the Darcy number. This is because of the larger bulk frictional resistance that the external flow experiences at the porous/fluid interface for a larger Darcy number. However, the peak values of C_f at the position corresponding to the right corner of each porous cavity increase as the Darcy number increases. Comparison of the Nusselt number distribution in Fig. 7(*b*) shows that at each permeable part of the wall (the inlet of cavity) the values of Nu_x decrease as the Darcy number decreases, while at the inner-cavity solid wall values of Nu_x increase as the Darcy number decreases. This is due to the lower velocity at the permeable part of wall and the higher velocity at the solid wall. These decreases and increases in the convective energy transport cause a lower temperature gradient and heat flux at the permeable wall, and a higher temperature gradient and heat flux at the solid wall, respectively.

Effect of the Prandtl Number. To study the effects of the Prandtl number on the flow and temperature fields, three different Prandtl numbers were chosen such that they will cover a wide range of thermophysical fluid properties. The numerical results are presented in Figs. 3, 8, and 9 for $Re_L = 3\times10^5$, $\Lambda_L = 0.35$, $Da_L = 8\times10^{-6}$, $A = 6$, and $B = 1$ for three different fluids with $Pr = 0.7$ (air), $Pr = 7$ (water), and $Pr = 100$ (some oil), respectively. Obviously, the Prandtl number variations have no effect on the flow field. However, as expected, the isotherms penetrate farther inside the porous cavities as Prandtl number decreases.

Inertial Effects. The inertial effects become noticeable when the Reynolds number based on the pore diameter becomes large. The effect of the inertial parameter is shown in Figs. 3 and 10 for $Re_L = 3\times10^5$, $Da_L = 8\times10^{-6}$, $Pr = 0.7$, $A = 6$, and $B = 1$ but $\Lambda_L = 0.35$ and 1.05, respectively. Comparison of the streamlines in Fig. 3(*a*) and 10(*a*) shows that as the inertial parameter increases, the strength of the vortices is reduced. This is due to the larger bulk frictional resistance for the flow,

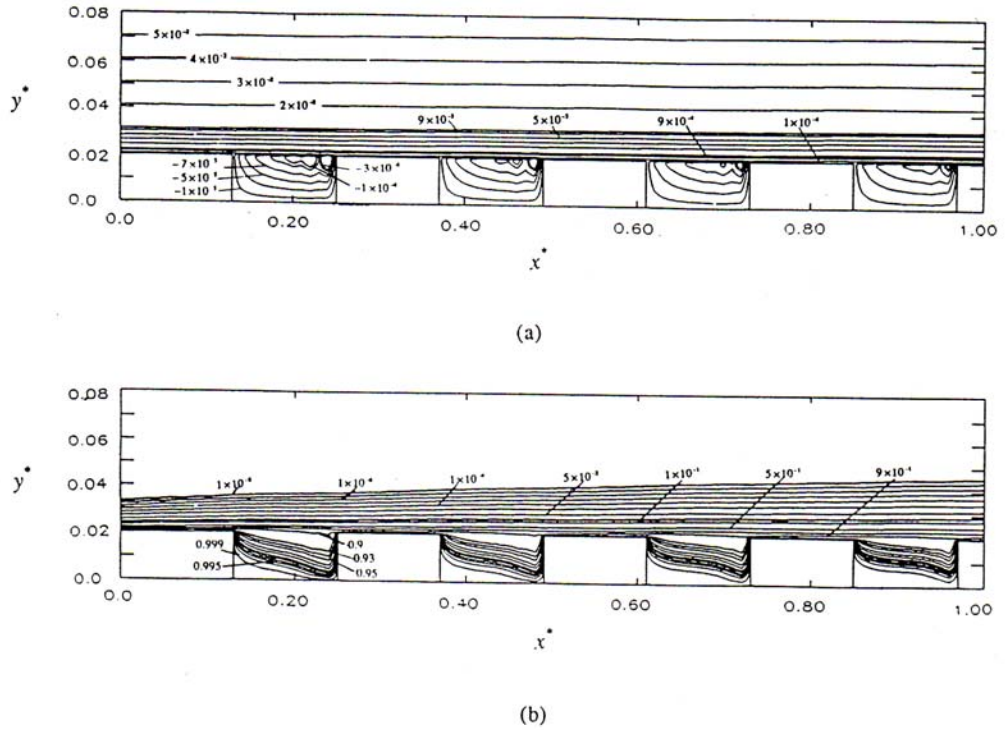

Fig. 6 (*a*) Streamlines and (*b*) isotherms for flow over four obstructing porous cavities for $Re_L = 3 \times 10^5$, $Da_L = 8 \times 10^{-6}$, $Pr = 0.7$, $k_{eff}/k_f = 1.0$, $\Lambda_L = 0.35$, $A = 6$, $B = 1$

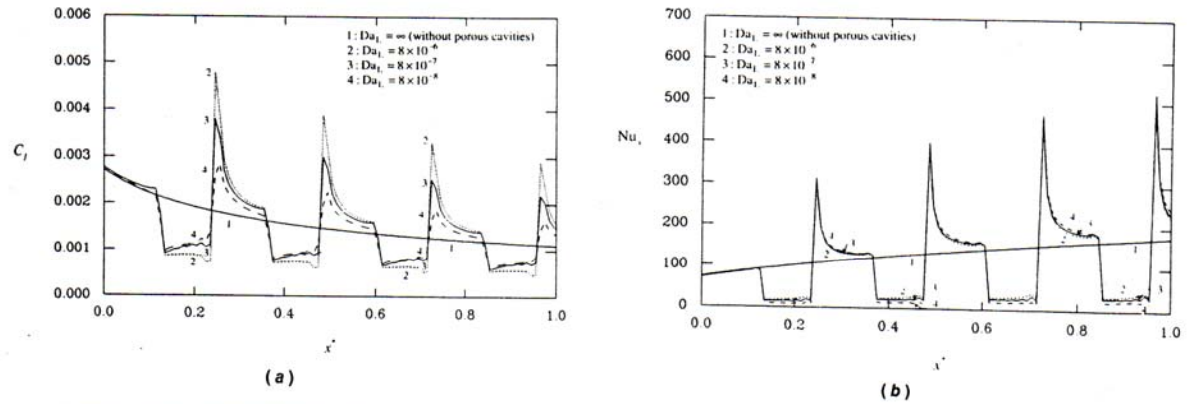

Fig. 7 Effects of the Darcy number on (*a*) friction coefficient and (*b*) Nusselt number for flow through alternate porous cavity-block obstacles for $Re_L = 3 \times 10^5$, $\Lambda_L = 0.35$, $Pr = 0.7$, $k_{eff}/k_f = 1.0$, $A = 3$, $B = 1$, $H^* = 0.02$

which the flow experiences at a larger inertial parameter. This in turn reduces the extent of penetration of the primary flow into the cavity. Comparison of the isotherms in Figs. 3(*b*) and 10(*b*) shows that for the smaller inertial parameter case the isotherms penetrate deeper into the cavity. This is owing to higher velocities for the smaller inertial parameter, which increases the transport of the convective energy. The above-described effects result in the friction coefficient and Nusselt number distributions shown in Fig. 11.

Effect of the First Geometric Parameter A. The effects of the aspect ratio (the first geometric parameter) A on the flow and temperature fields were studied for the general case of $Re_L = 3 \times 10^5$, $\Lambda_L = 0.35$, $Da_L = 8 \times 10^{-6}$, $Pr = 0.7$, and $B = 1$. The streamlines and isotherms for aspect ratios of $A = 3$ and 6 are presented in Figs. 12 and 3, respectively. As seen in Fig. 3 for $A = 6$ the flow in the cavity consists of a single laminar vortex that occupies the entire cavity. For $A = 3$ the flow is still characterized by a single vortex, but the vortex center is displaced toward the upstream cavity wall. This kind of flow situation may persist up to a certain value of A where the center of vortex just coincides with the center of cavity.

Effect of the Second Geometric Number B. The second geometric number $B = D^*/W^*$ reflects the influence of cavity array arrangement on the flow. There are two configurations considered in this analysis. The numerical runs were carried out for the general case of $Re_L = 3 \times 10^5$, $Da_L = 8 \times 10^{-6}$, $\Lambda_L = 0.35$, $Pr = 0.35$, and $A = 6$. When $A = 6$ and $B < 1$ the flow separates from the upstream top left corner of the first cavity,

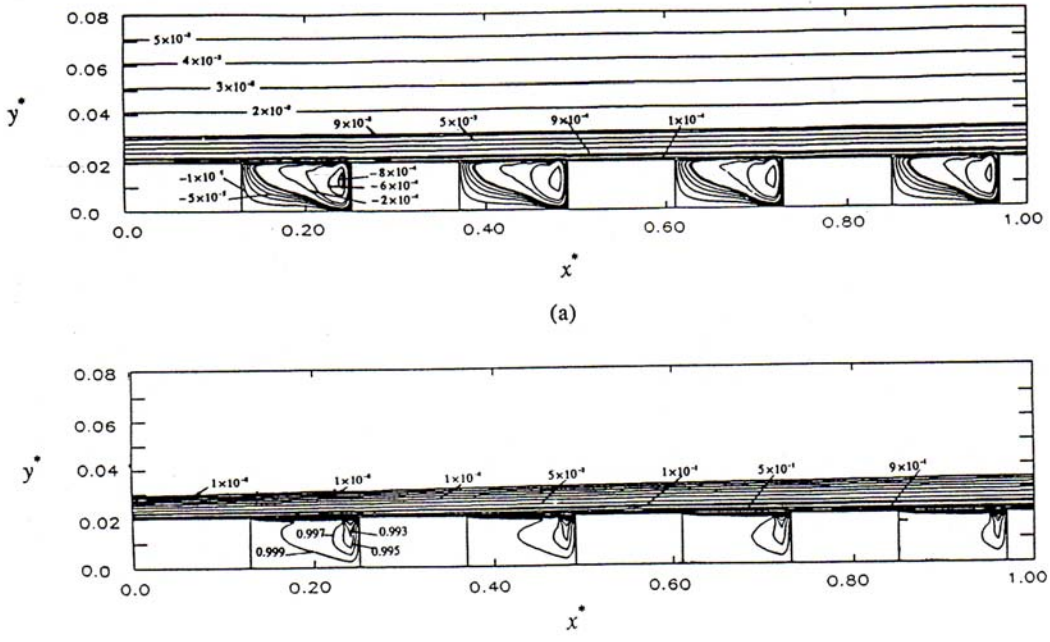

Fig. 8 (*a*) Streamlines and (*b*) isotherms for flow over four obstructing porous cavities for $Re_L = 3 \times 10^5$, $Da_L = 8 \times 10^{-6}$, $\Lambda_L = 0.35$, $Pr = 7$, $k_{eff}/k_f = 1.0$, $A = 6$, $B = 1$

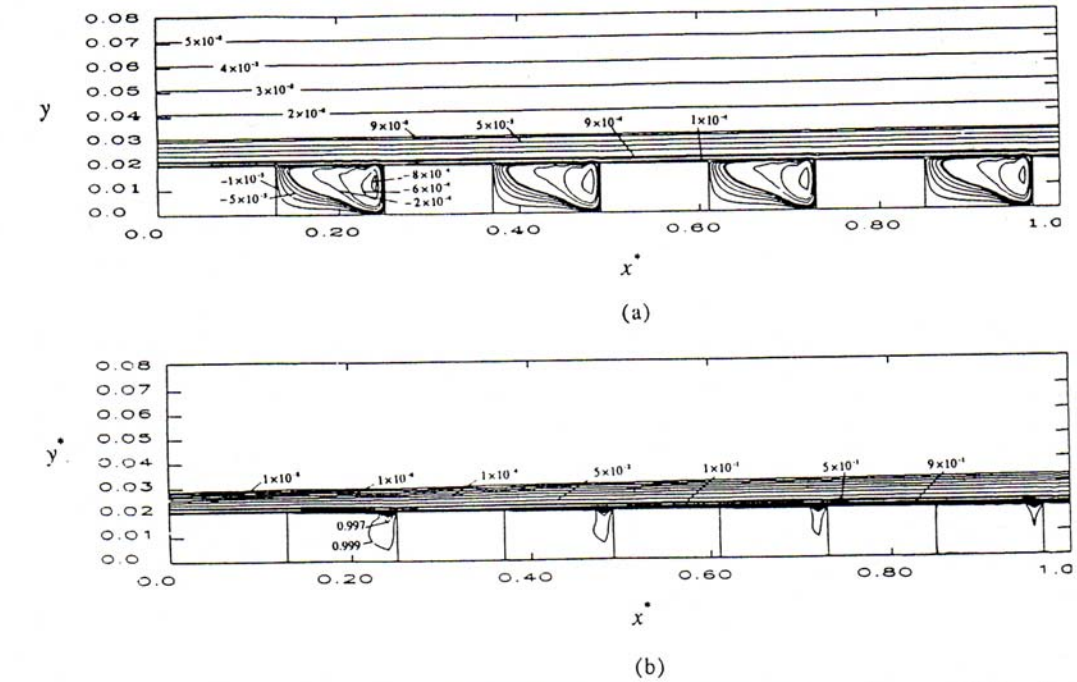

Fig. 9 (*a*) Streamlines and (*b*) isotherms for flow over four obstructing porous cavities for $Re_L = 3 \times 10^5$, $Da_L = 8 \times 10^{-6}$, $\Lambda_L = 0.35$, $Pr = 100$, $k_{eff}/k_f = 1.0$, $A = 6$, $B = 1$

reattaches on the bottom surface, and then reaches the downstream cavity wall. After passing through the first cavity the flow separates from the plate and an eddy region appears behind the separation point. This is due to a very steep velocity gradient (vorticity) in the fluid as it turns around the top right corner of the first cavity.

Under a special condition where both parameters A and B were changed, a few interesting results were found. When the value of A was decreased from 6 to 3 and B increased from 0.8 to 2, a secondary boundary layer started from the top right corner of the first cavity and was maintained over the external boundary between the first two cavities. This secondary boundary layer resulted in vortex flow inside the other three cavities. The reason for the appearance of the secondary boundary layer was that as the fluid turned around the top right corner of the first cavity, it experienced a milder velocity gradient. The ve-

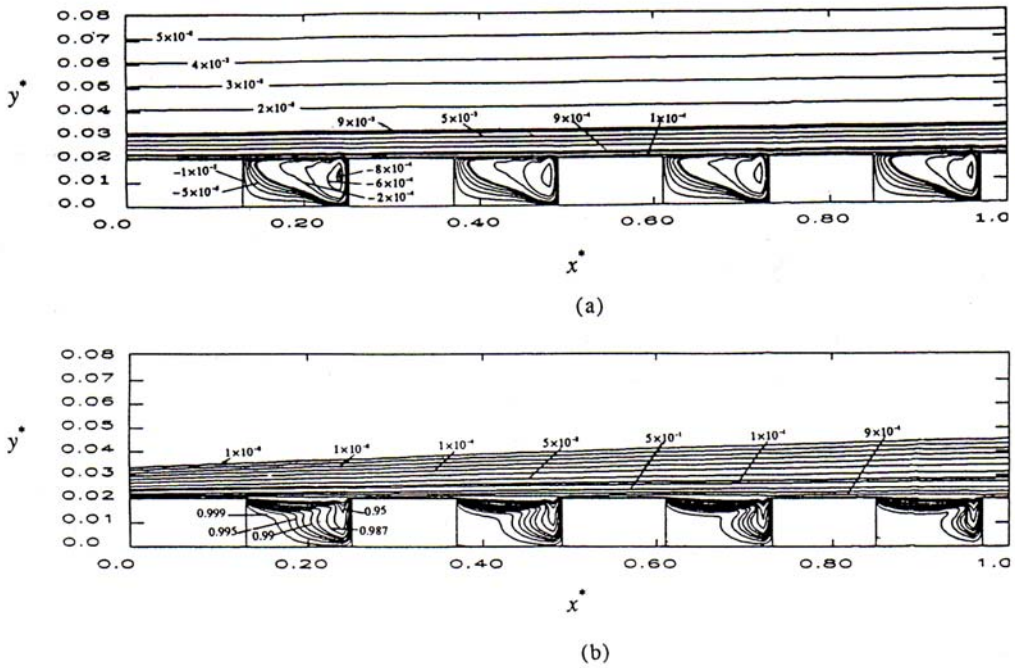

Fig. 10 (*a*) **Streamlines and** (*b*) **isotherms for flow over four obstructing porous cavities for** $Re_L = 3 \times 10^5$, $Da_L = 8 \times 10^{-6}$, $\Lambda_L = 1.05$, $Pr = 0.7$, $k_{eff}/k_f = 1.0$, $A = 6$, $B = 1$

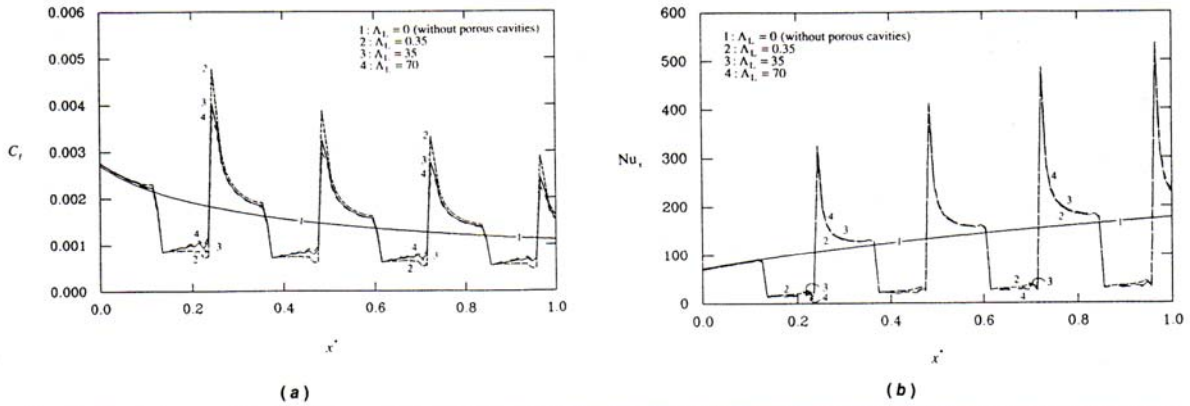

Fig. 11 The influence of the inertial parameter on (*a*) **friction coefficient and** (*b*) **Nusselt number for flow through alternate porous cavity-block obstacles for** $Re_L = 3 \times 10^5$, $Da_L = 8 \times 10^{-6}$, $Pr = 0.7$, $k_{eff}/k_f = 1.0$, $A = 3$, $B = 1$, $H^* = 0.02$

locity gradient was so small that the longitudinal pressure gradient was enough to reattach the flow to the wall. Comparison of the isotherms indicated that a reduction in the second geometric parameter B created a significant distortion of the isotherms. This is due to the separated and reattached flow regions, which were described previously. Finally, the streamlines and isotherms for the two-porous-cavity array were found to be very similar to those for the four-cavity array. It was found that the increase in the number of blocks has no substantial effect on the main features of the flow and temperature fields.

Conclusions

The main focus of this research is to analyze laminar forced convection over a composite porous/fluid system composed of multiple porous cavities. Since very little work has been done on external forced convection fluid flow and heat transfer in the composite systems, the objective of the present work is to study the interaction phenomena occurring in the porous medium and the fluid layer, and to analyze the effects of various parameters governing the physics of the problem under consideration. Characteristics of the flow and temperature fields in the composite layer and the effects of various governing dimensionless parameters, such as the Darcy number, Reynolds number, Prandtl number, the inertia parameter as well as the effects of pertinent geometric parameters were thoroughly analyzed and discussed. In addition, the interactive effects of the embedded porous substrates on skin friction and heat transfer characteristics of an external surface are analyzed. The fundamental information presented here can be extended to examine various applications such as in electronic cooling and in heat exchanger design, reduction of skin friction and heat transfer enhancement or augmentation, some of the manufacturing processes, geothermal reservoirs and oil extraction. The present work constitutes one of the first analyses of the laminar separated forced convection through porous cavities.

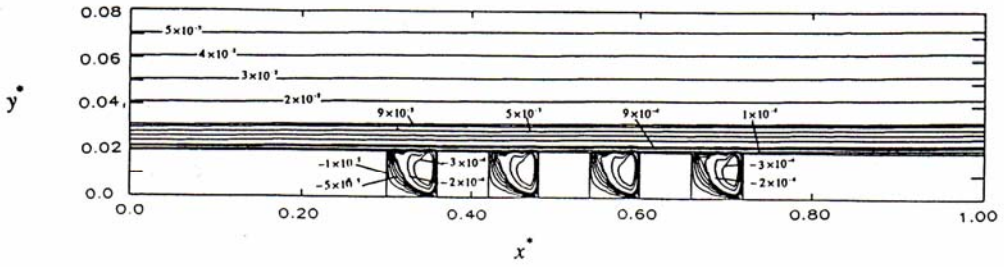

(a)

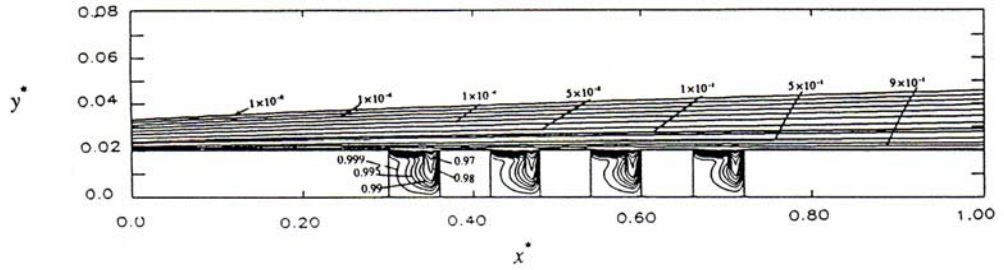

(b)

Fig. 12 (*a*) **Streamlines and** (*b*) **isotherms for flow over four obstructing porous cavities for** $Re_L = 3 \times 10^5$, $Da_L = 8 \times 10^{-6}$, $\Lambda_L = 0.35$, $Pr = 0.7$, $k_{eff}/k_f = 1.0$, $A = 3$, $B = 1$

Acknowledgments

A grant from OSC is acknowledged and appreciated.

References

Adams, J., and Ortega, J., 1982, "A Multicolor SOR Method for Parallel Computation," *Proceedings of Int. Conf. on Parallel Procession*, pp. 53–56.

Aung, W., 1983, "An Interferometric Investigation of Separated Forced Convection in Laminar Flow Past Cavities," ASME JOURNAL OF HEAT TRANSFER, Vol. 105, pp. 505–512.

Beckermann, C., Ramadhyani, S., and Viskanta, R., 1987, "Natural Convection Flow and Heat Transfer Between a Fluid Layer and a Porous Layer Inside a Rectangular Enclosure," ASME JOURNAL OF HEAT TRANSFER, Vol. 109, pp. 363–370.

Beckermann, C., Viskanta, R., and Ramadhyani, S., 1988, "Natural Convection in Vertical Enclosures Containing Simultaneously Fluid and Porous Layers," *J. Fluid Mech.*, Vol. 186, pp. 257–284.

Bejan, A., 1984, *Convection Heat Transfer*, Wiley, New York.

Bhatti, A., and Aung, W., 1984, "Finite Difference Analysis of Laminar Separated Forced Convection in Cavities," ASME JOURNAL OF HEAT TRANSFER, Vol. 106, pp. 49–54.

Cheng, P., 1978, "Heat Transfer in Geothermal System," *Adv. Heat Transfer*, Vol. 14, pp. 1–105.

De Vries, D. A., 1958, "Simultaneous Transfer of Heat and Moisture in Porous Media," *Transactions of American Geophysical Union*, Vol. 39, pp. 909–916.

Gooray, A. M., Watkins, C. B., and Aung, W., 1981, "Numerical Calculations of Turbulent Heat Transfer Downstream of a Rearward-Facing Step," *Proceedings of the 2nd International Conference on Numerical Method in Laminar and Turbulent Flow*, Venice, Italy, pp. 639–651.

Gooray, A. M., 1982, "Numerical Calculation of Turbulent Recirculating Heat Transfer Beyond Two-Dimension Backsteps and Sudden Pipe Expansion," Ph.D. Thesis, Mechanical Engineering Department, Howard University, Washington, DC.

Gooray, A. M., Watkins, C. B., and Aung, W., 1982, "K-ϵ Calculations of Heat Transfer in Redeveloping Turbulent Boundary Layers Downstream of Reattachment," ASME Paper No. 82-HT-77.

Gosman, A. D., 1976, "The TEACH-T Computer Program Structure, Flow, Heat and Mass Transfer in Turbulent Recirculating Flows—Prediction and Measurement," Lecture Notes from McGill University, Canada.

Greenspan, D., 1969, "Numerical Studies of Steady, Viscous, Incompressible Flow in a Channel With a Step," *J. Eng. Mathematics*, Vol. 3, No. 1, pp. 21–28.

Huang, P. C., and Vafai, K., 1993, "Flow and Heat Transfer Control Over an External Surface Using a Porous Block Array Arrangement," *Int. J. Heat Mass Transfer*, Vol. 36, pp. 4019–4032.

Patankar, S. V., 1980, *Numerical Heat Transfer and Fluid Flow*, Hemisphere, Washington, DC.

Poulikakos, D., and Bejan, A., 1985, "The Departure From Darcy Flow in Natural Convection in a Vertical Porous Layer," *The Physics of Fluids*, Vol. 28, pp. 3477–3484.

Poulikakos, D., 1986, "Buoyancy-Driven Convection in a Horizontal Fluid Layer Extending Over a Porous Substrate," *Phys. Fluids*, Vol. 29, pp. 3949–3957.

Poulikakos, D., and Kazmierczak, M., 1987, "Forced Convection in a Duct Partially Filled With a Porous Material," ASME JOURNAL OF HEAT TRANSFER, Vol. 109, pp. 653–662.

Roache, P. J., 1976, *Computational Fluid Dynamics*, Hermosa, Albuquerque, NM.

Sathe, S. B., Lin, W. Q., and Tong, T. W., 1988, "Natural Convection in Enclosures Containing an Insulation With a Permeable Fluid-Porous Interface," *Int. J. Heat Fluid Flow*, Vol. 9, pp. 389–395.

Sinha, S. N., Gupta, A. K., and Oberai, M. M., 1981, "Laminar Separating Flow Over Backsteps and Cavities—Part II: Cavities," *AIAA J.*, Vol. 20, No. 3, pp. 370–375.

Tien, C. L., and Vafai, K., 1989, "Convective and Radiative Heat Transfer in Porous Media," *Advances in Applied Mechanics*, Vol. 27, pp. 225–282.

Vafai, K., and Tien, C. L., 1981, "Boundary and Inertia Effects on Flow and Heat Transfer in Porous Media," *Int. J. Heat Mass Transfer*, Vol. 24, pp. 195–203.

Vafai, K., and Tien, C. L., 1982, "Boundary and Inertia Effects on Convective Mass Transfer in Porous Media," *Int. J. Heat Mass Transfer*, Vol. 25, pp. 1183–1190.

Vafai, K., and Thiyagaraja, R., 1987, "Analysis of Flow and Heat Transfer at the Interface Region of a Porous Medium," *Int. J. Heat Mass Transfer*, Vol. 30, pp. 1391–1405.

Vafai, K., and Kim, S. J., 1990, "Analysis of Surface Enhancement by a Porous Substrate," ASME JOURNAL OF HEAT TRANSFER, Vol. 112, pp. 700–705.

Yamamoto, H., Seki, N., and Fukusako, S., 1979, "Forced Convection Heat Transfer on Heated Bottom Surface of a Cavity," ASME JOURNAL OF HEAT TRANSFER, Vol. 101, pp. 475–479.